Natural Resources Canada | Ressources naturelles Canada

GEOLOGICAL SURVEY OF CANADA
OPEN FILE 7649

# Geochemistry of regional surficial sediment samples from the Thelon River to the East Arm of Great Slave Lake, Northwest Territories, Canada

B.A. Kjarsgaard, A.P. Plourde, R.D. Knight, and D.R. Sharpe

2014

Canada


**GEOLOGICAL SURVEY OF CANADA**
**OPEN FILE 7649**

# Geochemistry of regional surficial sediment samples from the Thelon River to the East Arm of Great Slave Lake, Northwest Territories, Canada

**B.A. Kjarsgaard[1], A.P. Plourde[2], R.D. Knight[1], D.R. Sharpe[1]**

[1] Geological Survey of Canada, Ottawa, Ontario
[2] University of Ottawa, Ottawa, Ontario

## 2014



doi:10.4095/295195

This publication is available for free download through GEOSCAN (http://geoscan.nrcan.gc.ca/).

**Recommended citation**
Kjarsgaard, B.A., Plourde, A.P., Knight, R.D., and Sharpe, D.R., 2014. Geochemistry of regional surficial sediment samples from the Thelon River to the East Arm of Great Slave Lake, Northwest Territories, Canada; Geological Survey of Canada, Open File 7649, 1 zip file. doi:10.4095/295195

Publications in this series have not been edited; they are released as submitted by the author.

## 1.0 Introduction

This report integrates geochemical data for surficial sediment samples (till), previously released for the Thaidene Nene MERA study area, (Kjarsgaard et al., 2013a) and the adjacent Operation GEM Mary Francis Lake – Whitefish Lake – Thelon River study area (Kjarsgaard et al., 2013b). This region, in the southeast part of the Northwest Territories, spans the transition from northern boreal forest in the south and southwest to barrenlands tundra in the north and northeast. The combined data set contains 400 till samples analysed for the <0.063 mm size fraction by three different digestion methods (aqua regia, 4-acid, lithium borate/tetraborate fusion) followed by Inductively Coupled Plasma Mass Spectrometry/ Emission Spectrometry (ICP-MS/ES) analysis and 346 analyses for the <2 mm size fraction, analysed by two different digestion methods (4-acid, lithium borate/tetraborate fusion) followed by ICP-MS/ES analysis. Note that the <2 mm size fraction of the 2009 till samples for the MERA project were not analysed. All analytical data are presented in Appendix A. All sample locations are shown in Figure 1.

## 2.0 Sample collection, processing and analytical methods

Till sample sites were determined based on a 10 km x 10 km grid (Kjarsgaard et al., 2013b, c), resulting in approximately one sample per 100 $km^2$ (Fig. 1). A greater sample density exists in the northwest part of the study area, as 2009 follow-up work investigated a gold grain anomaly observed in till and esker heavy mineral samples from 2008 sampling (Kerr et al., 2013a). Additional sampling in 2009 to the east and west of Artillery Lake was also undertaken to follow-up on two kimberlite indicator mineral anomalies reported in industry assessment files (Kjarsgaard, 2013a). The 2012 sampling was undertaken as part of a regional surficial project for Operation GEM, as a follow-up to the MERA study, which delineated a significant chromite – olivine – Cr-diopside dispersal train (Kjarsgaard 2013b; Kjarsgaard et al., 2013c; Knight et al., 2013), whose source was further east of the eastern border of the MERA area.

At each site two till samples were collected, a 1 kg sample for geochemistry, and an additional 10 to 15 kg sample for heavy mineral analysis. The 1 kg sample was sent to Acme Analytical Laboratories Ltd. (Acme), Vancouver, B.C. for processing (drying, sieving to <0.063 mm, and to <2mm fractions), and laboratory geochemical analyses. Geochemistry data for the clay-silt size fraction (<0.063 mm), was determined by ICP-ES/MS analyses following each of lithium borate fusion (fusion), 4-acid, and aqua-regia digestion methods (Kjarsgaard et al., 2013a), while data for the <2 mm size fraction was determined by ICP-ES/MS analysis after lithium borate fusion, and 4-acid digestion. Details of the analytical methods and certified reference material standards utilized are presented in Kjarsgaard et al. (2013a, 2013b, 2014). A complete listing of elements analysed, and their detection limits, for all three methods is presented in Table 1. For the

2012 till samples, rare earth element (REE) concentrations were not determined for the <0.063 mm size fraction following the aqua regia digestion. This was based on results from the 2008 and 2009 MERA data sets (see Kjarsgaard et al., 2013b, 2014), which illustrated that REE data acquired after aqua regia partial digestion did not provide additional useful information with respect to REE data from the 4-acid or fusion digestions.

Single element maps (Appendix B) of the data were produced using a Natural Neighbour interpolation of Vertical Mapper operating within MapInfo™, with a cell length of 100 m and an aggregation distance of 500 m. For trace elements, the colour profile was fixed for the $0^{th}$, $50^{th}$, $95^{th}$, $98^{th}$ and $100^{th}$ percentiles, allowing better resolution in areas with anomalously high concentrations. For major elements the colour profile was fixed for the $0^{th}$, $20^{th}$, $80^{th}$, $98^{th}$, and $100^{th}$ percentiles, which provided a compromise between resolution of the regional geochemical trends and resolution in areas with anomalously high concentrations.

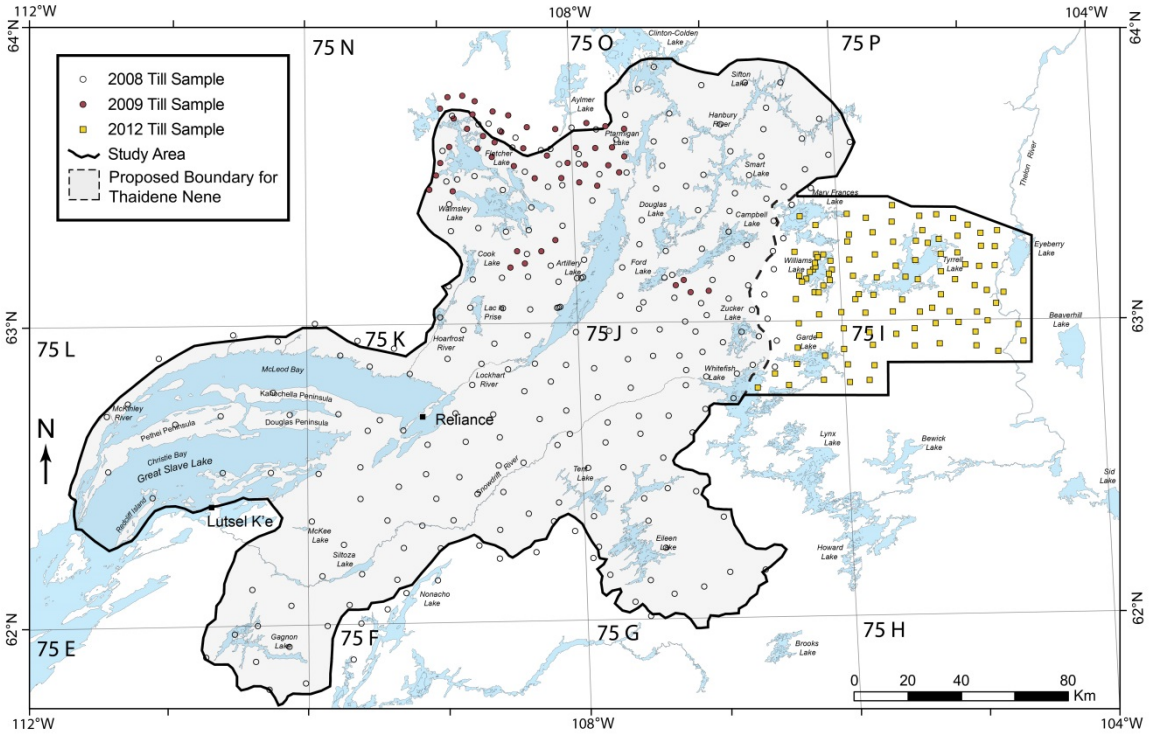


Figure 1. Outline of the study area, with site locations for till geochemistry.

| **FUSION** | | | **4 Acid** | | | **Aqua regia** | | |
|---|---|---|---|---|---|---|---|---|
| Element | Unit | MDL | Element | Unit | MDL | Element | Unit | MDL |
| SiO2 | % | 0.01 | Ti | % | 0.001 | Ti | % | 0.001 |
| TiO2 | % | 0.01 | Al | % | 0.02 | Al | % | 0.01 |
| Al2O3 | % | 0.01 | Fe | % | 0.02 | Fe | % | 0.01 |
| Cr2O3 | % | 0.002 | Ca | % | 0.02 | Mg | % | 0.01 |
| Fe2O3 | % | 0.04 | Mg | % | 0.02 | Ca | % | 0.01 |
| MnO | % | 0.01 | Na | % | 0.002 | Na | % | 0.001 |
| MgO | % | 0.01 | K | % | 0.02 | K | % | 0.01 |
| CaO | % | 0.01 | P | % | 0.001 | P | % | 0.001 |
| Na2O | % | 0.01 | S | % | 0.04 | S | % | 0.02 |
| K2O | % | 0.01 | Li | ppm | 0.1 | Li | ppm | 0.1 |
| P2O5 | % | 0.01 | Rb | ppm | 0.1 | Rb | ppm | 0.1 |
| LOI | % | 0.10 | Cs | ppm | 0.1 | Cs | ppm | 0.02 |
| TOT/C | % | 0.02 | Be | ppm | 1 | Be | ppm | 0.1 |
| TOT/S | % | 0.02 | Ba | ppm | 1 | Sr | ppm | 0.5 |
| Rb | ppm | 0.1 | Sr | ppm | 1 | Ba | ppm | 0.5 |
| Cs | ppm | 0.1 | Zr | ppm | 0.2 | Zr | ppm | 0.1 |
| Be | ppm | 1 | Nb | ppm | 0.04 | Nb | ppm | 0.02 |
| Sr | ppm | 0.5 | Hf | ppm | 0.02 | Hf | ppm | 0.02 |
| Ba | ppm | 1 | Ta | ppm | 0.1 | Ta | ppm | 0.05 |
| Zr | ppm | 0.1 | Y | ppm | 0.1 | Y | ppm | 0.01 |
| Nb | ppm | 0.1 | Sc | ppm | 0.1 | Sc | ppm | 0.1 |
| Hf | ppm | 0.1 | V | ppm | 1 | V | ppm | 2 |
| Ta | ppm | 0.1 | Cr | ppm | 1 | Cr | ppm | 0.5 |
| Y | ppm | 0.1 | Mn | ppm | 2 | Mn | ppm | 1 |
| Sc | ppm | 1 | Co | ppm | 0.2 | Co | ppm | 0.1 |
| V | ppm | 8 | Ni | ppm | 0.1 | Ni | ppm | 0.1 |
| Cr | ppm | 14 | Cu | ppm | 0.02 | Cu | ppm | 0.01 |
| Co | ppm | 0.2 | Zn | ppm | 0.2 | Zn | ppm | 0.1 |
| Ni | ppm | 20 | Pb | ppm | 0.02 | Pb | ppm | 0.01 |
| Cu | ppm | 5 | Mo | ppm | 0.05 | Tl | ppm | 0.02 |
| Zn | ppm | 5 | W | ppm | 0.1 | Mo | ppm | 0.01 |
| Pb | ppm | 1 | As | ppm | 0.2 | W | ppm | 0.1 |
| Mo | ppm | 1 | Sb | ppm | 0.02 | As | ppm | 0.1 |
| W | ppm | 0.5 | Bi | ppm | 0.04 | Sb | ppm | 0.02 |
| Ga | ppm | 0.5 | Ga | ppm | 0.02 | Bi | ppm | 0.02 |
| Sn | ppm | 1 | Cd | ppm | 0.02 | B | ppm | 20 |
| La | ppm | 0.1 | Sn | ppm | 0.1 | Se | ppm | 0.1 |
| Ce | ppm | 0.1 | La | ppm | 0.1 | Te | ppm | 0.02 |
| Pr | ppm | 0.02 | Ce | ppm | 0.02 | Ga | ppm | 0.1 |
| Nd | ppm | 0.30 | Pr | ppm | 0.1 | Ge | ppm | 0.1 |
| Sm | ppm | 0.05 | Nd | ppm | 0.1 | Cd | ppm | 0.01 |
| Eu | ppm | 0.02 | Sm | ppm | 0.1 | Sn | ppm | 0.1 |
| Gd | ppm | 0.05 | Eu | ppm | 0.1 | In | ppm | 0.02 |
| Tb | ppm | 0.01 | Gd | ppm | 0.1 | La | ppm | 0.5 |
| Dy | ppm | 0.05 | Tb | ppm | 0.1 | Ce | ppm | 0.1 |
| Ho | ppm | 0.02 | Dy | ppm | 0.1 | Pr | ppm | 0.02 |
| Er | ppm | 0.03 | Ho | ppm | 0.1 | Nd | ppm | 0.02 |
| Tm | ppm | 0.01 | Er | ppm | 0.1 | Sm | ppm | 0.02 |
| Yb | ppm | 0.05 | Tm | ppm | 0.1 | Eu | ppm | 0.02 |
| Lu | ppm | 0.01 | Yb | ppm | 0.1 | Gd | ppm | 0.02 |
| Th | ppm | 0.2 | Lu | ppm | 0.1 | Tb | ppm | 0.02 |
| U | ppm | 0.1 | Th | ppm | 0.1 | Dy | ppm | 0.02 |
| | | | U | ppm | 0.1 | Ho | ppm | 0.02 |
| | | | Au | ppm | 0.1 | Er | ppm | 0.02 |
| | | | Ag | ppb | 20 | Tm | ppm | 0.02 |
| | | | | | | Yb | ppm | 0.02 |
| | | | | | | Lu | ppm | 0.02 |
| | | | | | | Th | ppm | 0.1 |
| | | | | | | U | ppm | 0.1 |
| | | | | | | Pd | ppb | 10 |
| | | | | | | Ag | ppb | 2 |
| | | | | | | Re | ppb | 1 |
| | | | | | | Pt | ppb | 2 |
| | | | | | | Au | ppb | 0.2 |
| | | | | | | Hg | ppb | 5 |

Table 1. Listing of elements analysed, units of measurement, and their detection limits for Fusion, 4-Acid, and Aqua Regia methods. MDL (minimum detection limit).

## 3.0 Bedrock Geology

The study area spans six major geological domains (Fig. 2; Kjarsgaard et al., 2013d). The Archean Slave Craton, located in the northwest, consists of granite, metaturbidite, and volcanic rocks with minor gneiss, and mafic and alkaline intrusives. In the southeast the Archean and Paleoproterozoic Rae domain of the Churchill Province consists of gneiss and granitoid with minor mafic plutons and volcanic rocks, and clastic sequences of the Nonacho Group. The Slave Craton is separated from the Rae domain of the Churchill Province by the Thelon tectonic zone and the Talston magmatic zone. The Thelon consists dominantly of ortho- and para-gneiss with granitoids, and minor mafic intrusions. The Taltson comprises granite with granitoid mylonite, gneissic rocks, and mafic intrusions. The Paleoproterozoic East Arm basin contains a range of clastic sedimentary sequences, as well as carbonates (some stromatolitic), and minor mafic to felsic volcanic rocks and associated intrusions.

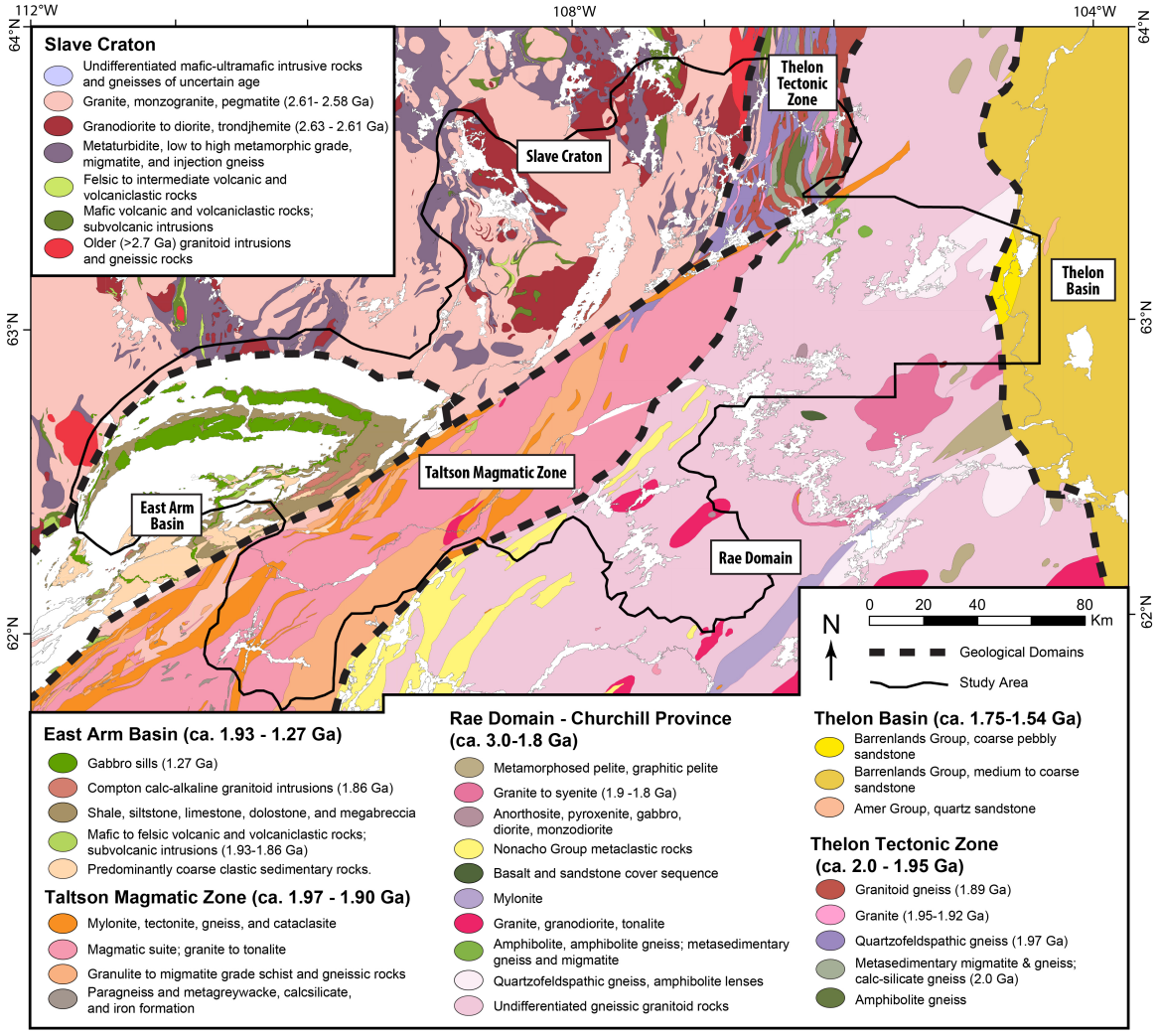


Figure 2. Generalized and simplified bedrock geology map based on a 1: 250,000 scale compilation by Kjarsgaard et al. (2013d) with additions from Kjarsgaard et al. (2013b).

The eastern edge of the study area hosts the Paleoproterozoic Thelon Basin, consisting dominantly of sandstone and pebbly sandstone of the Barrenlands Group. These rocks overlie sandstone and pelite of the Amer Group (Pehrsson et al., 2014). Other than small areas mapped in detail by industry adjacent to the Thelon River, the bedrock geology of the Rae domain is poorly understood, based on mapping at 1:1-million scale (Wright, 1967), with revisions by Pehrsson et al. (2014) and additional updating by Kjarsgaard (Fig. 2).

## 4. Mineralization

The region from the Thelon River to the East Arm hosts numerous mineral showings (Fig. 3). Studies by Roscoe et al. (1987) noted the occurrence of gold, uranium and base metal mineralization styles and also iron formation in the region of Artillery Lake and the East Arm of Great Slave Lake. Kjarsgaard et al. (2013e) provided a classification of ~500 mineral occurrences within the MERA study area, which utilized the Decade of North America (DNAG) classification system of Eckstrand et al. (1996). An additional style of mineralization not present in the MERA study area is known from Boomerang Lake, which lies approximately 20 km south of the southeast limit of the study area (Fig. 3). The Boomerang Lake deposit is interpreted as unconformity-related U mineralization, with associated Au, Ag, and base metals, +/- PGEs (Davidson and Gandhi, 1989; Beyer et al., 2010).

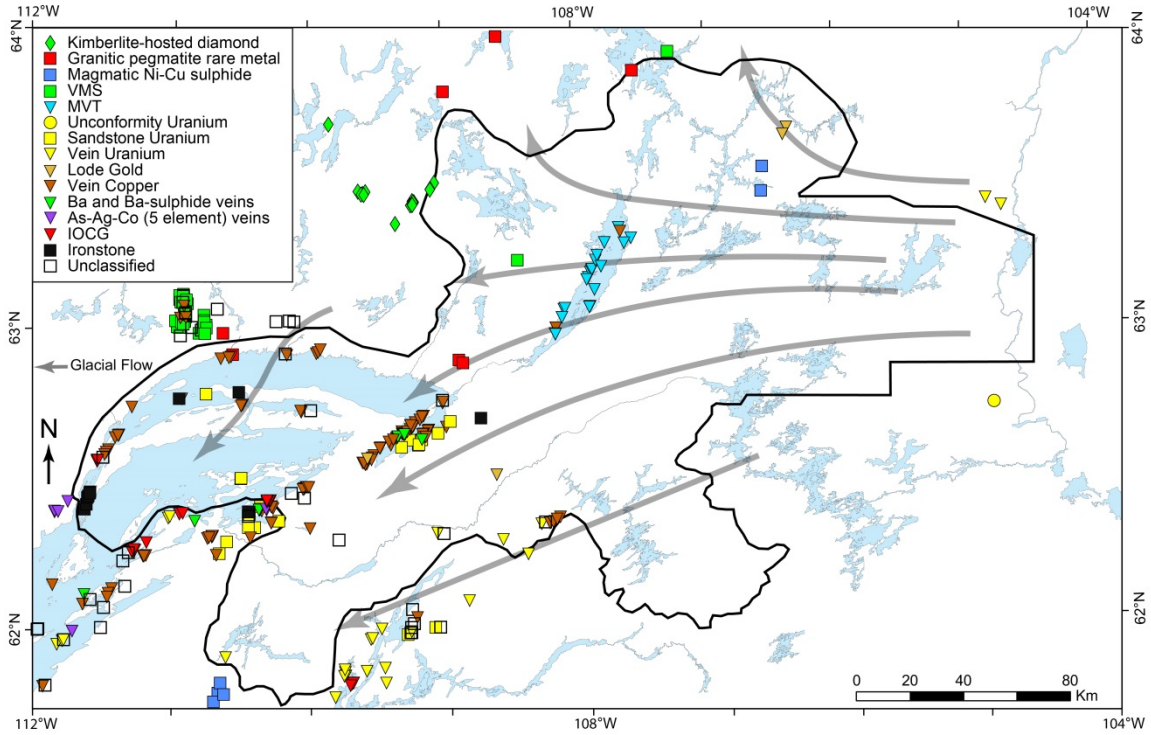


Figure 3. Mineral showings by type (Kjarsgaard et al. 2013e), within and adjacent to the study area, with dominant glacial flow direction shown by grey arrows (see Fig. 4 fort details).

Fourteen types of mineralisation are recognized within or directly adjacent to the present study area, including: kimberlite-hosted diamond; granite pegmatite rare metal; magmatic Ni-Cu sulphide; volcanogenic massive sulphide (VMS) and Mississippi Valley type (MVT) base metal; sandstone, unconformity and vein uranium; lode gold; vein copper; silver-arsenide-cobalt ("5-element") vein; iron oxide copper gold (IOCG); ironstone, and Ba, Ba-sulphide vein (Fig. 3). The MERA report (Wright et al., 2013) contains individual chapters that describe each mineralization style in more detail, with the exception of unconformity U, as at Boomerang Lake.

## 5. Surficial Geology

The study area lies in the Keewatin Sector of the former Laurentide Ice Sheet, west of the Keewatin Ice Divide (Lee et al., 1957). This region spans the transition from northern boreal forest in the southwest to barrenlands tundra in the northeast. The main mapped glacial flow direction indicators in the area display an east to west, radiating pattern (Fig. 4), as first noted by Aylsworth and Shilts (1989), related to the latest glacial events. A sparse northeast to southwest flow direction was also observed the study area, but it is not significant in terms of sediment transport; transport is dominated by the east to west radial flow (Fig. 4; Sharpe et al., 2013, 2014; Kerr et al., 2013b). The east – west glacial flow fans out to a southwest trend in the southern and western part of the study area, and trends northwest in the northern part of the study area (Fig. 4). Surficial deposits in the region are dominated by sediment sourced from the Thelon Basin. Quartz sand, from weathered quartz sandstone of the Thelon Basin, was dispersed throughout the study area by the westward radial glacial flow. As a result, the proportion and thickness of the surficial sediment decreases from east to west (Fig. 5). The till is a matrix-supported, sandy diamicton, which decreases in quartz sand content east to west (Kjarsgaard et al., 2013a, b; Sharpe et al., 2014; unpublished data of the authors), moving away from the quartz-rich sandstone source in the Thelon Basin (see Fig. 2). Geochemically, Thelon Basin-sourced quartz results in significant $SiO_2$ concentrations in diamicton, with at least 50% of the study area having significant quartz influx, corresponding to the red (>94 wt% $SiO_2$), and yellow and light green (>77 wt% $SiO_2$) areas in Figure 6. The high levels of quartz sand in the east also resulted in the formation of more abundant and larger eskers than in the western part of the study area, although a regularly spaced (~10 km) network of eskers spans the entire region (Sharpe et al., 2013, 2014). Details (i.e., size, geometry) of surficial landforms throughout the region e.g., erosion forms, drumlins, crag-and-tails, esker/bedrock corridors, eskers, hummocks, transverse ridges, terraces and strandlines are documented in Sharpe et al. (2013, 2014).

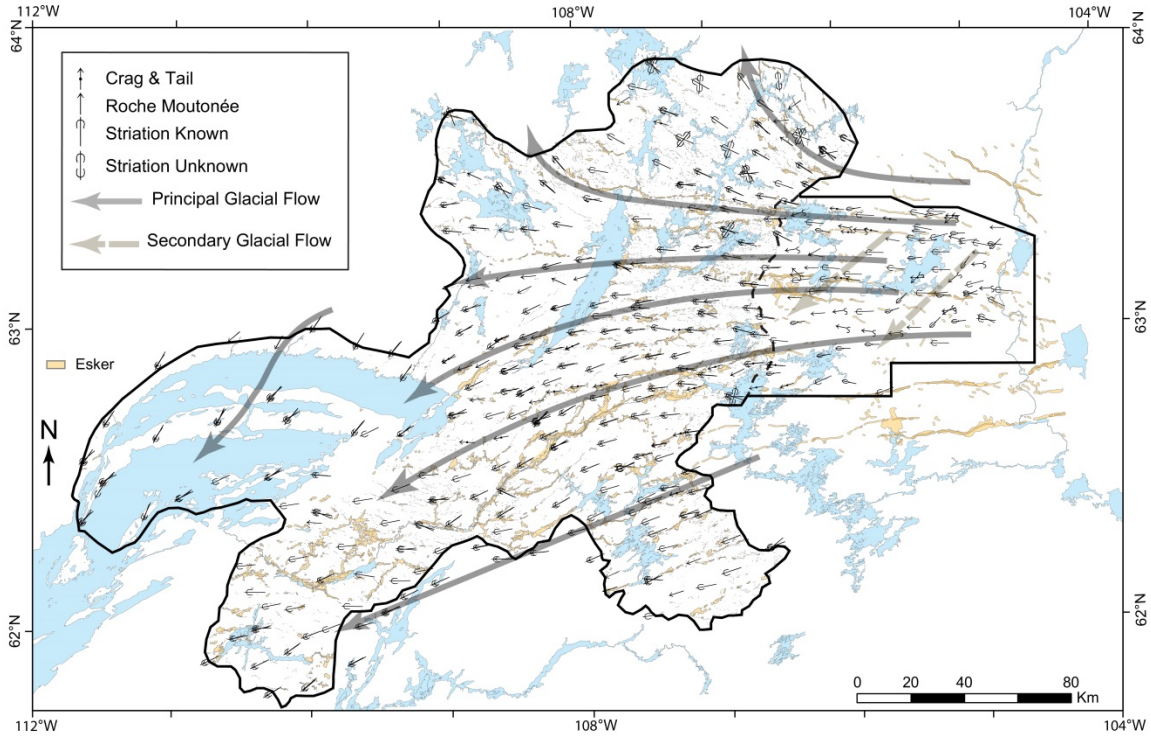


Figure 4. Detailed and principal glacial flow features of the study area. Data for the eastern part of the study area from Sharpe et al. (2014) and the western and central regions from Sharpe et al. (2013) that incorporates data from Kerr et al. (2013c).

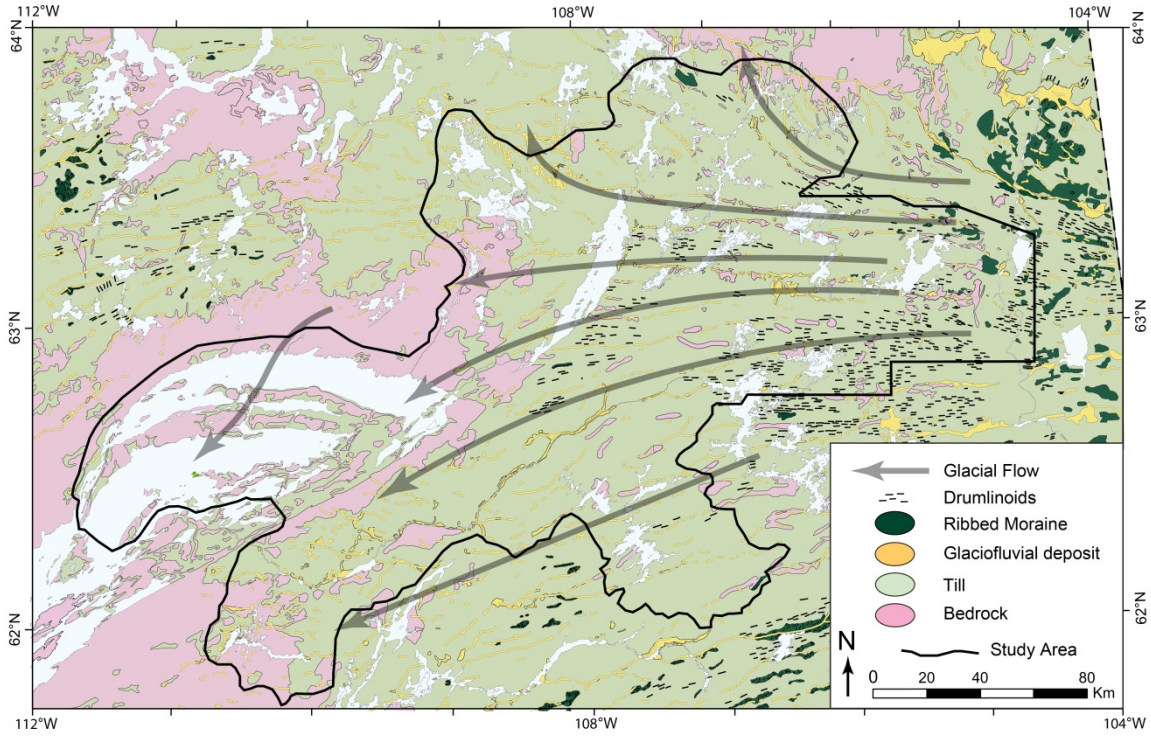


Figure 5. Generalized surficial geology (after Aylsworth and Shilts, 1989) with the principle glacial flow direction from Figure 4.

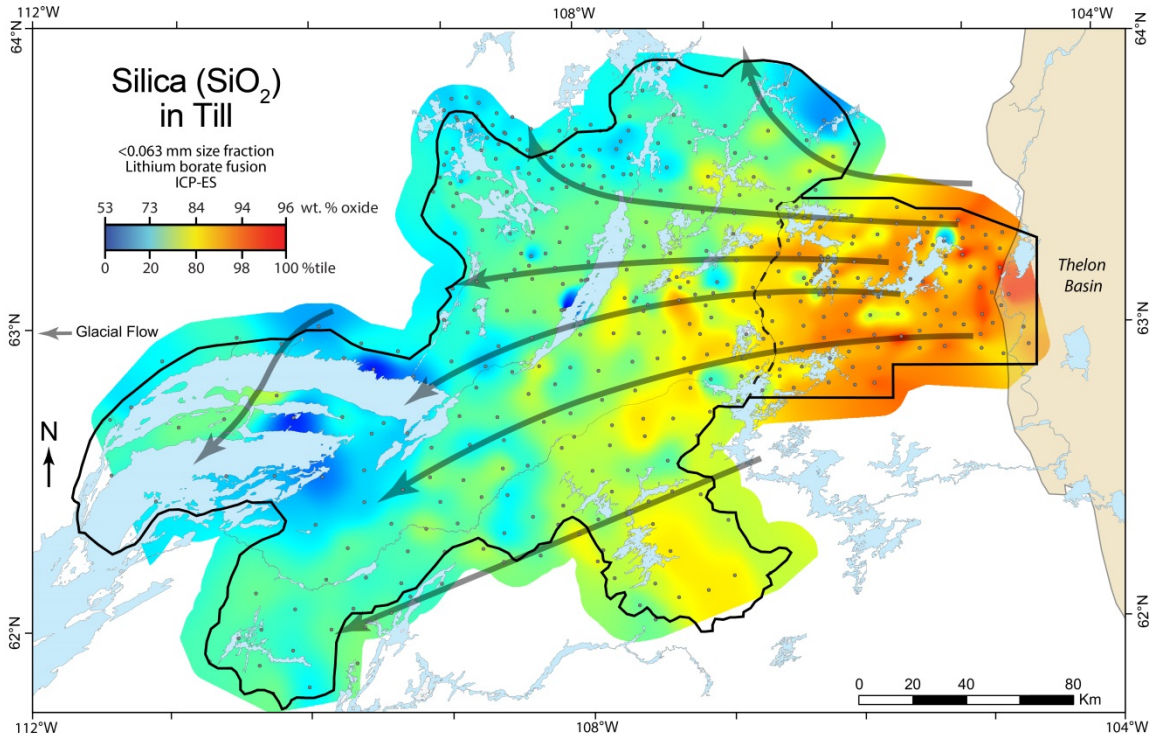


Figure 6. Interpolated surface depicting the concentration of silica (wt% $SiO_2$) in till samples, illustrating the high levels of silica adjacent to the Thelon Basin quartz sandstone source rocks. Silica concentration levels in till decrease from the east to the west, down-flow and away from the source.

## 6.0 Till geochemistry for mineral exploration

The till geochemical data set is presented in Appendix A. Single element interpolated geochemical maps are presented in Appendix B, with a listing of the interpolated maps in Table 2. These maps are based on a percentile scale and the range of concentration for any element may differ for each map, depending on the analytical method utilized (and hence the detection limit), as well as the maximum concentration level, which changes for some elements depending upon the grain size analysed. For the <0.063 mm and <2 mm size fraction, interpolated maps were generated for both fusion and 4-acid digestion data. Interpolated maps for aqua regia where produced only for the <0.063 mm size fraction, as this digestion method was not utilized on the <2 mm data, following on the rationale described in Kjarsgaard et al. (2014).

| Fusion | 4 Acid | Aqua regia |
|---|---|---|
| $SiO_2$ | Cr | Bi |
| $TiO_2$ | Co | Sn |
| $Al_2O_3$ | Ni | Pt |
| $Fe_2O_3$ | Cu | Au |
| MgO | Zn | As |
| CaO | Pb | |
| $Na_2O$ | Sb | |
| $K_2O$ | Cd | |
| $P_2O_5$ | Ag | |
| Rb | Li | |
| Cs | | |
| Ba | | |
| Zr | | |
| Nb | | |
| Hf | | |
| Ta | | |
| Y | | |
| Mn | | |
| V | | |
| Cr | | |
| Co | | |
| Ni | | |
| Ce | | |
| Nd | | |
| Dy | | |
| Yb | | |
| Lu | | |
| Th | | |
| U | | |

Table 2. Listing of single element maps generated for <0.063 mm and <2 mm size fractions of till for fusion and 4-acid data, and for aqua regia data (<0.063 mm size fraction of till).

We note that interpretation of aqua regia data may be misleading for many elements, as it is only a partial dissolution (e.g., see Kjarsgaard et al., 2014). As an example, Figure 7 displays bivariate plots of Ba concentration as a function of the three analytical methods utilized. While fusion and 4-acid have a strong correlation ($r^2 = 0.978$) and a near-perfect 1:1 fit, the aqua regia data has much lower concentration levels than either the fusion or 4-acid data, and consequently has poor correlations with either fusion or 4-acid data ($r^2 = 0.176$, and 0.173, respectively). While this effect is especially pronounced with Ba, other elements show similar behaviour. Concentrations determined by the fusion and 4-acid methods are generally similar, however, a subset of elements such as Cr (Fig. 8) and Zr have higher concentration values by fusion, which is due to incomplete digestion of chromite/Cr-spinel and zircon grains, respectively, by the 4-acid method.

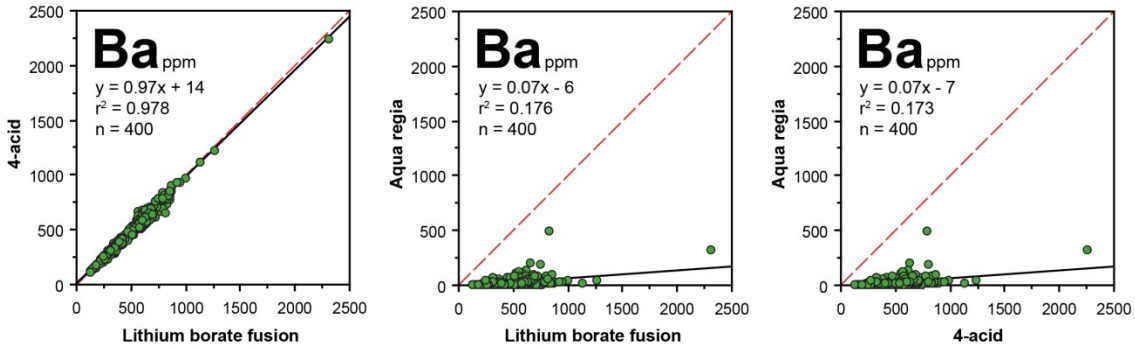


Figure 7. Comparison of barium concentrations (<0.063 mm size fraction) for three methods: 4-acid vs. fusion; aqua regia vs. fusion; aqua regia vs. 4-acid.

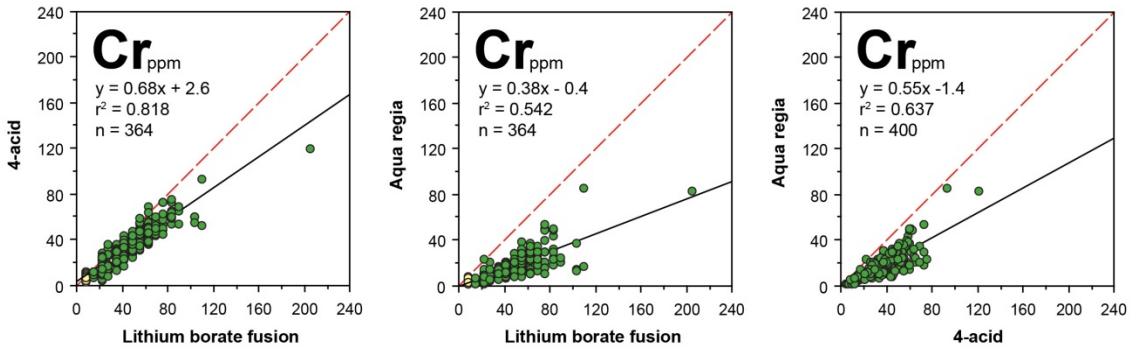


Figure 8. Comparison of chromium concentrations (<0.063 mm size fraction) for three methods: 4-acid vs. fusion; aqua regia vs. fusion; aqua regia vs. 4-acid.

A highly important aspect of the till geochemistry in the study area is the recognition that the eastern most till samples are extremely silica-rich (>94 wt% $SiO_2$), with silica content decreasing to the west (Fig. 6). From an exploration perspective, there are two basic principles of the application of surficial sediment geochemistry to mineral exploration that are worth noting: 1) the target 'ore' source material will be diluted when it is mixed with a regional sediment, which decreases the geochemical signal of the target. With further transport down-ice, additional dilution continues to lower the target signature as more regional sediment is incorporated, and; 2) the higher the concentration is for any specific ore pathfinder element of interest in the regional sediment, the more difficult it will be to detect the target 'ore' source for that element, as the local sediment provides a geochemical mask. While geochemical masking is an important factor in surficial mineral exploration studies, it is often not considered. In the present study, geochemical masking has a negligible effect in the eastern part of the study area, where till is dominated by quartz from the Thelon Basin sandstone i.e., the local till is nearly pure $SiO_2$. Exceptions to this are the elements Zr and Hf, which are of high concentration levels in the zircon-

rich quartz sandstone, and the till derived from it (Fig. 9). The observation that the regional till only masks for Zr and Hf, suggests that target anomalies for any other elements in the surficial sediments should in fact be easier, and not more difficult to detect in the study area, if one can account for the large quartz ($SiO_2$) dilution effect.

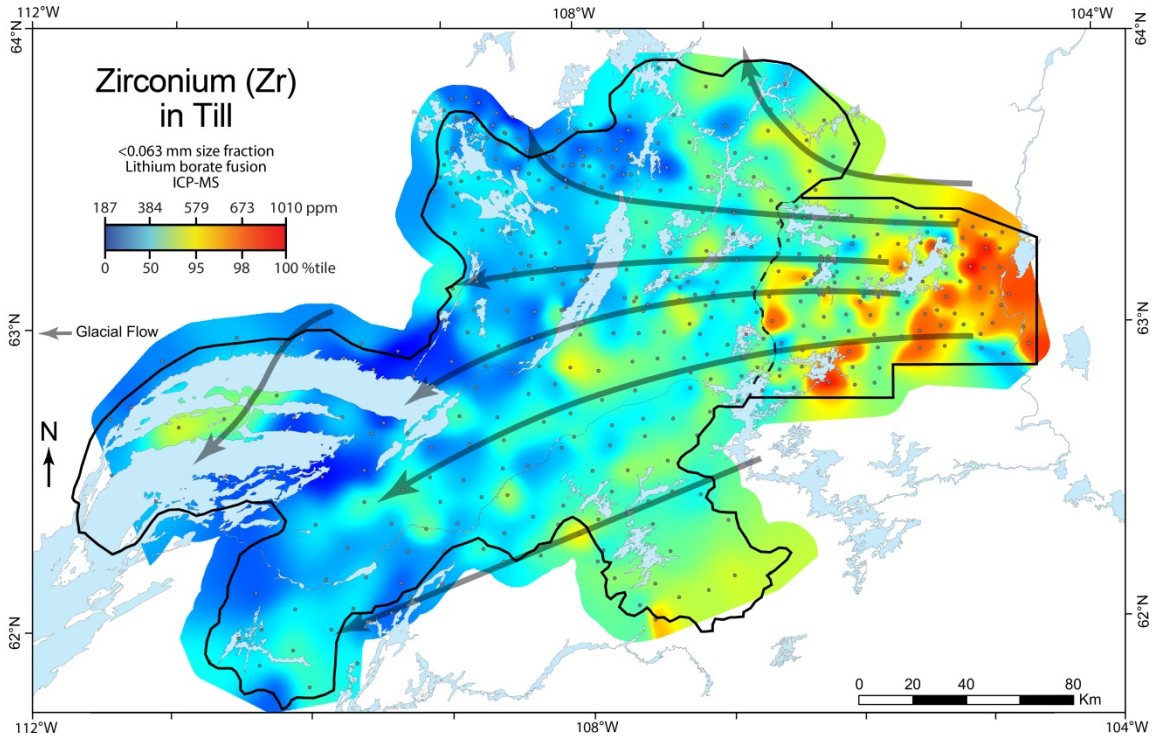


Figure 9. Interpolated surface depicting the concentration of Zr in till for the <0.063 mm size fraction. Note the general similarity of the Zr interpolated surface to that for silica shown in Figure 6, i.e., high concentrations in the east and lower concentrations in the west.

To test this theory we utilize a simple, but elegant transform of the raw data to produce $SiO_2$ "normalized" element maps. From a mineralogical perspective, we are eliminating the silica dilution resulting from the large influx of quartz grains from the Thelon Basin that is entrained in the regional sediment (till). The mathematical expression utilized is:

$$A_{norm}(x) = A(x)\frac{1-\overline{SiO_2}}{1-SiO_2(x)}$$

Where the elemental concentration A(x), at a given sample x, is divided by one minus its silica concentration $SiO_2(x)$ in order to remove the effect of $SiO_2$ dilution. The value is also multiplied by a scaling factor of one minus the median $SiO_2$ concentration for all samples in the study area.

We utilize the element chromium (via fusion digestion) for the dilution test. For comparison, picked mineral grain results for chromite from till and esker heavy mineral samples are shown in Figure 10. A large chromite anomaly with the highest concentration of picked grains occurs ~10 km east of Williams Lake, and grain counts decrease down-flow (Fig. 10). There is a known Cr till geochemistry anomaly (Fig. 11; see also Kjarsgaard et al., 2013a), but it does not correspond to the picked grain anomaly - it is smaller and lies mainly to the west of Williams Lake. However, when the silica transform is applied to the raw Cr data, the "$SiO_2$ normalized" Cr map exhibits an anomaly that is much more extensive (compare Figs. 11 and 12), and perhaps more importantly, extends to the east side of Williams Lake. The eastern edge of the anomaly on the "$SiO_2$ normalized" Cr map (Fig. 12) is now spatially coincident to that of the chromite indictor mineral map (Fig. 10), i.e., east of Williams Lake, and suggested to be near-source. The significant improvement of the Cr anomaly by using the transform demonstrates that accounting for dilution by regional sediment will assist mineral exploration programs in recognizing and finding the 'ore' source target. Furthermore, this transform technique could also be used to find or refine geochemical anomalies that are hidden or obscured by a combination of geochemical masking and dilution processes.

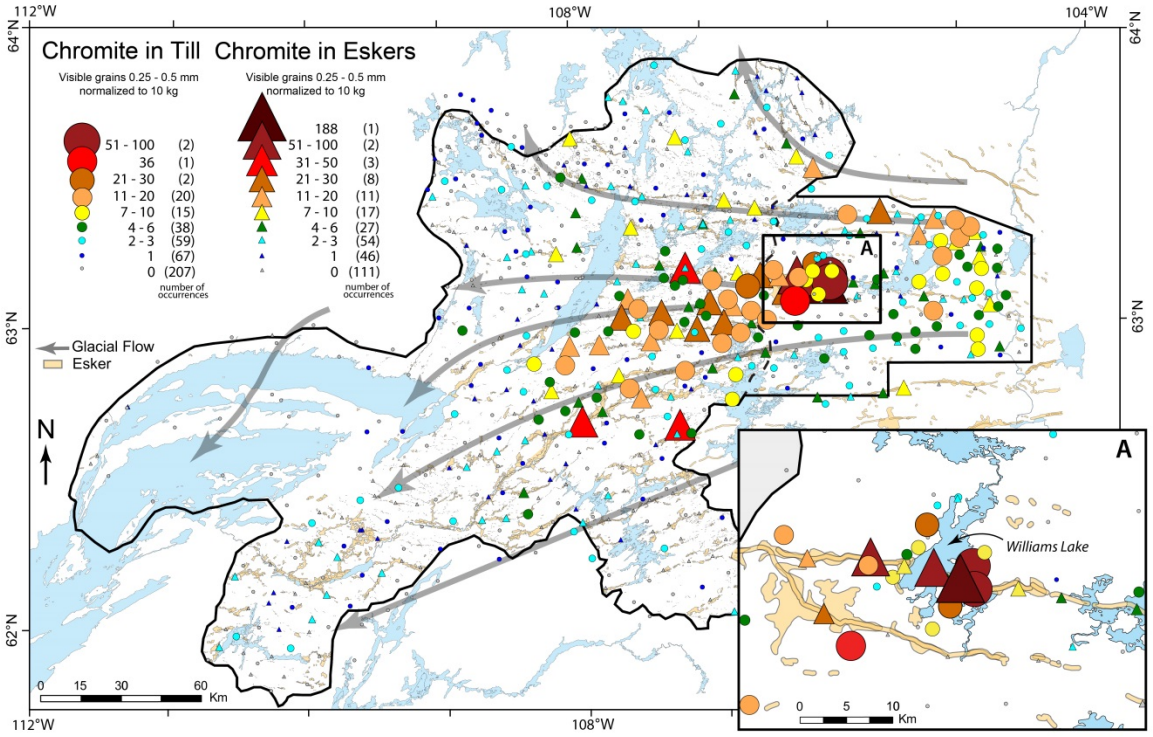


Figure 10. Chromite indicator mineral dispersal train in the study area (data from Kjarsgaard et al., 2013c and Knight et al., 2013). Inset map 'A' displays mineral grain counts adjacent to Williams Lake in greater detail.

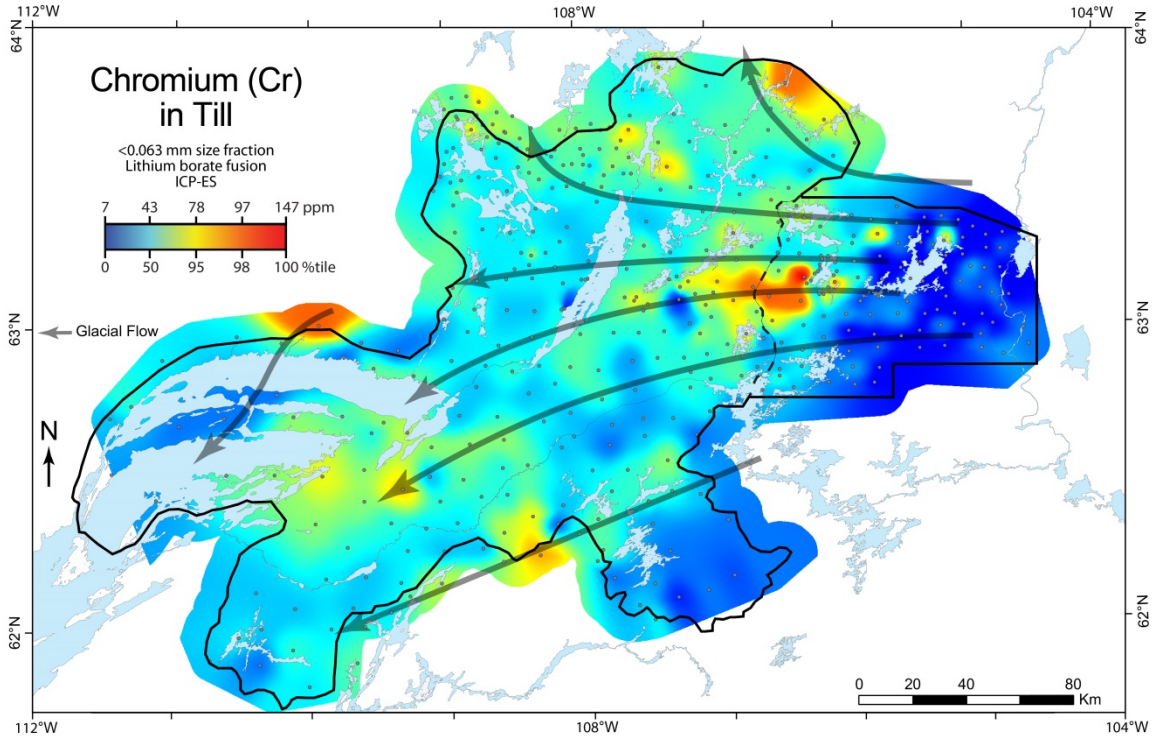


Figure 11. Interpolated surface depicting the concentration of Cr in till for the < 0.063 mm size fraction. Note the head of the main Cr anomaly lies west of Williams Lake.

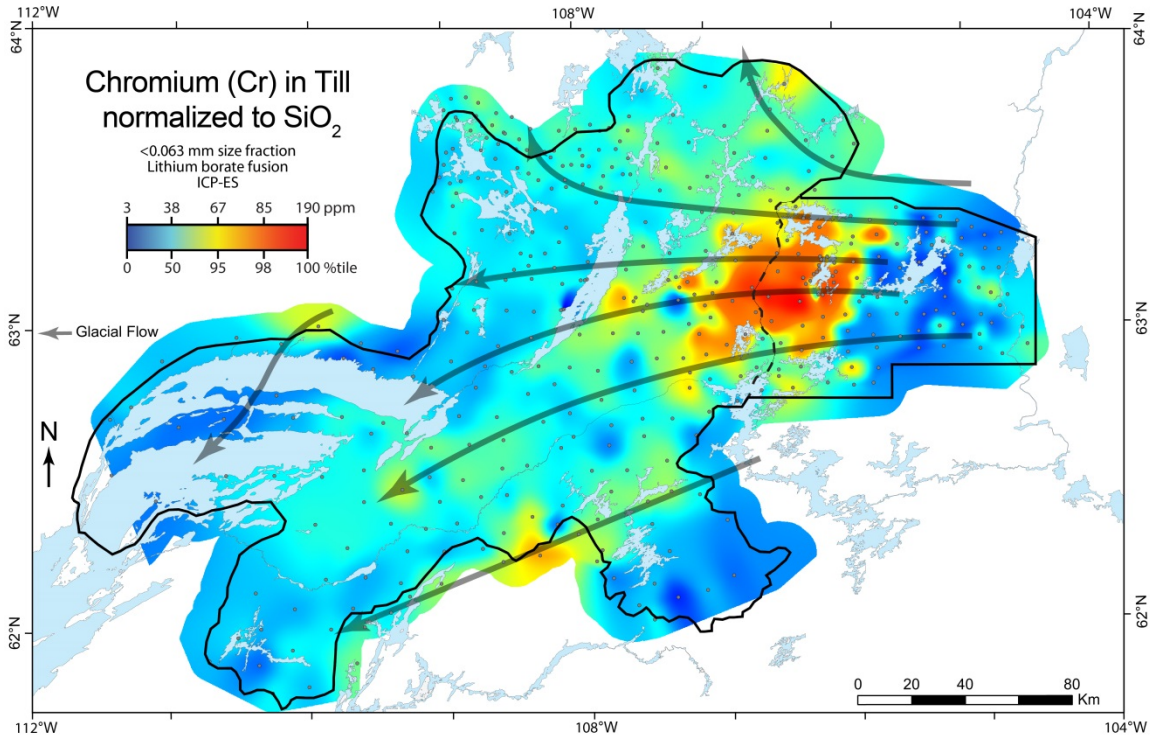


Figure 12. Interpolated surface depicting the concentration of Cr in till with the effect of $SiO_2$ dilution removed using the silica transform (see text for details). Note that the head of the main Cr anomaly lies to the west of Williams Lake and is coincident with the head of the chromite heavy mineral anomaly (see Fig. 10).

## 7.0 Acknowledgements

Stephen Day is thanked for his careful review, which proved very helpful. Brief, but insightful discussions with Eric Grunsky regarding preliminary tactics to address the dilution effects of the silica- and quartz-rich tills were greatly appreciated.

## 8.0 References

Aylsworth, J.M and Shilts W.W. (1989). Glacial Features Around the Keewatin Ice Divide: Districts of Mackenzie and Keewatin. Geological Survey of Canada, Map 24-1987, scale 1:1 000 000.

Beyer, S.R., Kyser, K., Hiatt, E.E. and Fraser, I. (2010). Geological evolution and exploration geochemistry of the Boomerang Lake unconformity-type uranium prospect, Northwest Territories, Canada *in* Goldfarb, R.J., Marsh, E.E., and Monecke, T. (eds.). The challenge of finding new mineral resources: global metallogeny, innovative exploration, and new discoveries. Society of Economic Geologists Special Publication, #15, v. 2: Zinc-lead, nickel-copper-PGE, and uranium, p. 675-702.

Davidson, G.I. and Gandhi, S.S. (1989). Unconformity-related U-Au mineralization in the middle Proterozoic Thelon sandstone, Boomerang lake prospect, Northwest Territories, Canada. Economic Geology, v. 84, p. 143-157.

Eckstrand, O.R., Sinclair, W.D. and Thorpe, R. (1996). Geology of Canadian Mineral Deposit Types. Geological Survey of Canada, Geology of Canada, no. 8, 640 p.

Kerr, D.E., Knight, R.D., Sharpe, D.R., Cummings, D.I. and Kjarsgaard, B.A., and Russell, H.A.J. (2013a). Gold grain counts from till and esker samples in the proposed national park reserve, East Arm of Great Slave Lake *in* Mineral and Energy Resource Assessment for the Proposed Thaidene Nene National Park Reserve in the Area of the East Arm of Great Slave Lake Northwest Territories, D.F. Wright, E.J. Ambrose, D. Lemkow and G.F. Bonham-Carter (eds.). Geological Survey of Canada, Open File 7196, p. 191-259.

Kerr, D.E., Knight, R.D., Sharpe, D.R., Cummings, D.I., Russell, H.A.R. and Kjarsgaard, B.A. (2013b). Surficial geology of the proposed national park reserve on the East Arm of Great Slave Lake *in* Mineral and Energy Resource Assessment for the Proposed Thaidene Nene National Park Reserve in the area of the East Arm of Great Slave Lake, Northwest Territories, D.F. Wright, E.J. Ambrose, D. Lemkow

and G.F. Bonham-Carter (eds.). Geological Survey of Canada, Open File 7196, p. 143-154.

Kerr, D.E., Knight, R.D., Sharpe, D.R., Cummings, D.I. and Kjarsgaard, B.A. (2013c). Surficial geology map, East Arm MERA study area, scale 1:250,000 *in* Mineral and Energy Resource Assessment for the Proposed Thaidene Nene National Park Reserve in the area of the East Arm of Great Slave Lake, Northwest Territories, D.F. Wright, E.J. Ambrose, D. Lemkow and G.F. Bonham-Carter (eds.). Geological Survey of Canada, Open File 7196, Digital Supplement 2.

Kjarsgaard, B.A. (2013a). Potential for kimberlite-hosted diamond occurrences, Thaidene Nene MERA study area *in* Mineral and Energy Resource Assessment for the Proposed Thaidene Nene National Park Reserve in the Area of the East Arm of Great Slave Lake, Northwest Territories, D.F. Wright, E.J. Ambrose, D. Lemkow and G.F. Bonham-Carter (eds.). Geological Survey of Canada, Open File 7196, p. 339-348.

Kjarsgaard, B.A. (2013b). Potential for chromite mineralization, East Arm of Great Slave Lake *in* Mineral and Energy Resource Assessment for the Proposed Thaidene Nene National Park Reserve in the Area of the East Arm of Great Slave Lake, Northwest Territories, D.F. Wright, E.J. Ambrose, D. Lemkow and G.F. Bonham-Carter (eds.); Geological Survey of Canada, Open File 7196, p. 349-356.

Kjarsgaard, B.A., Knight, R.D., Grunsky, E.C., Kerr, D.E., Sharpe, D.R., Cummings, D.I., Russell, H.A.J., Kerswill, J.A., and Wright, D.F. (2013a). Till geochemistry studies of the Thaidene Nene MERA study area *in* Mineral and Energy Resource Assessment for the Proposed Thaidene Nene National Park Reserve in the area of the East Arm of Great Slave Lake, Northwest Territories, D.F. Wright, E.J. Ambrose, D. Lemkow and G.F. Bonham-Carter (eds.); Geological Survey of Canada, Open File 7196, p. 313-337.

Kjarsgaard, B.A., Knight, R., Plourde, A.P., Sharpe, D. R. and Lesemann, J.-E. (2013b). Geochemistry of till samples, NTS 75-I, 75-J, 75-O, 75-P (Mary Frances Lake – Whitefish Lake – Thelon River area), Northwest Territories. Geological Survey of Canada, Open File 7351, 28 p. and 3 digital appendices.

Kjarsgaard, B.A., Knight, R.D., Sharpe, D.R., Kerr, D.E., Cummings, D.I., Russell, H.A.J., and Lemkow, D. **(**2013c). Significance of indicator minerals from till and esker samples, Thaidene Nene MERA study area *in* Mineral and Energy Resource Assessment for the Proposed Thaidene Nene National Park Reserve in the Area of the East Arm of Great Slave Lake, Northwest Territories, D.F. Wright, E.J.

Ambrose, D. Lemkow and G.F. Bonham-Carter (eds.); Geological Survey of Canada, Open File 7196, p. 279-312.

Kjarsgaard, B.A., Lemkow, D. and Tella, S. (2013d). Bedrock geology map, East Arm MERA study area, scale 1:250 000. *in* Mineral and Energy Resource Assessment for the Proposed Thaidene Nene National Park Reserve in the area of the East Arm of Great Slave Lake, Northwest Territories, D.F. Wright, E.J. Ambrose, D. Lemkow and G.F. Bonham-Carter (eds.). Geological Survey of Canada, Open File 7196, Digital supplement 1.

Kjarsgaard, B.A., Potter, E., Ghandi, S.S., Lydon, J., Jefferson C. and Kerswill, J. (2013e). Mineral deposit classification for 499 MERA mineral occurrences *in* Mineral and Energy Resource Assessment for the Proposed Thaidene Nene National Park Reserve in the area of the East Arm of Great Slave Lake, Northwest Territories, D.F. Wright, E.J. Ambrose, D. Lemkow and G.F. Bonham-Carter (eds.). Geological Survey of Canada, Open File 7196, Digital Supplement 3, MERA mineral-occurrences.shp

Kjarsgaard, B.A., Knight, R.D., Plourde, A.P. and Reynen, A.M.G. (2014). Portable XRF spectrometry of surficial sediment samples in the region of East Arm, Great Slave Lake, Northwest Territories, Canada; Geological Survey of Canada, Open File 7607.

Knight, R.D., Kjarsgaard, B.A., Plourde, A.P., Sharpe, D.R. and Lesemann, J-E. (2013). Significance of indicator minerals from till and esker samples, NTS 75I, 75J, 75O, 75P (Mary Frances Lake – Whitefish Lake– Thelon River area). Geological Survey of Canada, Open File 7540.

Lee, H.A., Craig, B.G. and Fyles, J.G. (1957). Keewatin Ice Divide. Geological Society of America Bulletin, v. 68, p. 1760-1761.

Pehrsson, S.J., Currie, M., Ashton, K., Harper, C., Paul, D., Pana, D., Berman, R., Bostock, H., Corkery, T., Jefferson, C.W., and Tella, S. (2014). Bedrock geology compilation and regional synthesis of south Rae and parts of Hearne domains, Churchill Province, Northwest Territories, Saskatchewan, Nunavut, Manitoba and Alberta. Geological Survey of Canada, Open File 5744, scale 1:550 000.

Sharpe, D.R., Russell, H.A.J. and Knight, R.D. (2013). Glaciofluvial features and their significance in the proposed national Park Reserve, East Arm of Great Slave Lake *in* Mineral and Energy Resource Assessment for the Proposed Thaidene Nene National Park Reserve in the area of the East Arm of Great Slave Lake, Northwest

Territories, D.F. Wright, E.J. Ambrose, D. Lemkow and G.F. Bonham-Carter (eds.). Geological Survey of Canada, Open File 7196, p. 155-190.

Sharpe, D.R., Lesemann, J-E., Knight, R., Kjarsgaard, B.A. and Plourde, A.P., (2014). Glacial landscape architecture and sediment sampling, Mary Frances Lake – Whitefish Lake – Thelon River area (NTS 75-I, 75-J, 75-O, 75-P), Northwest Territories. Geological Survey of Canada, Open File 7554.

Wright D.F., Ambrose, E.J., Lemkow, D. and G.F. Bonham-Carter, G.F. (2013). Mineral and Energy Resource Assessment for the Proposed Thaidene Nene National Park Reserve in the area of the East Arm of Great Slave Lake, Northwest Territories. Geological Survey of Canada, Open File 7196.

Wright, G.M., 1967. Southeastern barren grounds. Geological Survey, Map 1261A. Scale 1:1 000 000.